

Supplementary Information

SrVO₃-Modified Silver Nanowires Transparent Conductive Film with Enhanced Photoelectric Performance and Optical Stability

Li GAN^{a,b}, Ying LIU^{a,c}, Xiaojiao YANG^{a,c}, Wanxia HUANG^a, Ningjia YANG^a, Yibo NIU^a, Xin TIAN^{a,*}

^a*College of Materials Science and Engineering, Sichuan University, Chengdu 610065, China*

^b*Chongqing Xiyu New Material Technology Co., Ltd., Chongqing 401420, China*

^c*Key Laboratory of Advanced Special Materials and Technology, Ministry of Education, Chengdu
610065, China*

* Corresponding author: Xin TIAN.

E-mail address: tianxin.990@scu.edu.cn (Xin TIAN).

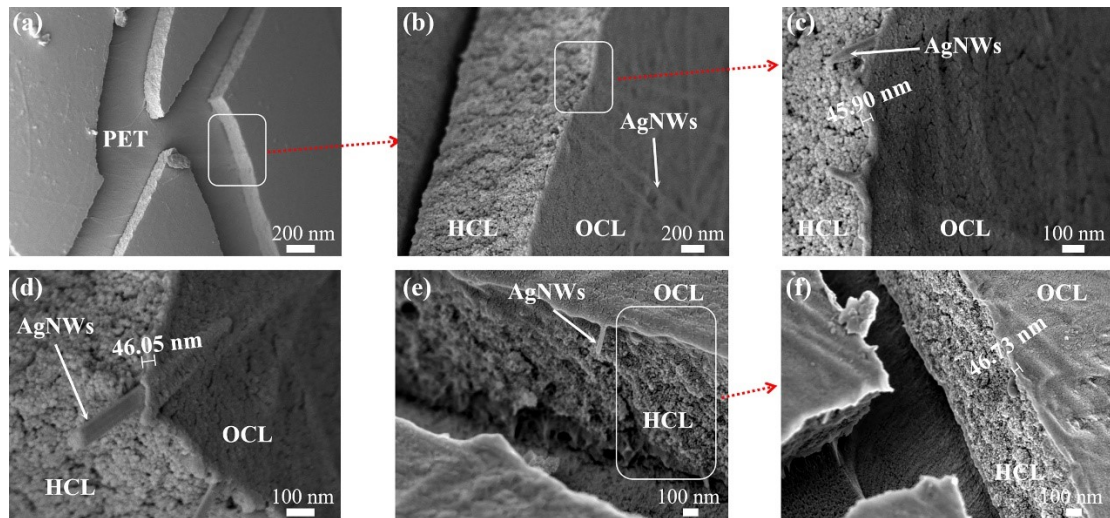


Fig. S1 Cross-sectional SEM micrographs of the coatings: (a) TCF0 (total coating thickness: 45.90 nm), (b) TCF10 (46.05 nm), and (c) TCF20 (46.73 nm). All coatings exhibit well-controlled thicknesses within the narrow range of 45~47 nm, demonstrating precise thickness control in the single-factor experiments.

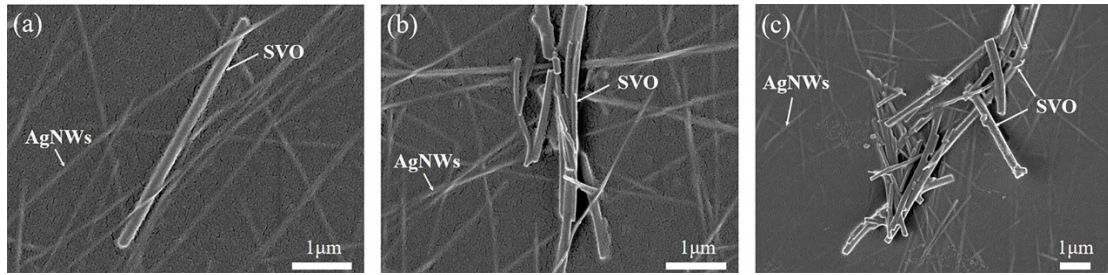


Fig. S2 Morphological characterization of SVO distribution in ANCL-encapsulated transparent conductive films: (a) Optimally doped TCF10 (0.010 wt% SVO) showing uniform dispersion, (b) Highly concentrated TCF15 (0.015 wt%) and (c) TCF20 (0.020 wt%) systems, revealing concentration-dependent aggregation behavior.

Comprehensive XPS spectral analysis was conducted to elucidate the optical and chemical stability characteristics of SVO nanofibers. The overlapped core-level spectra (O 1s + V 2p) under varying UV irradiation durations (0, 500, and 1000 h) are presented in Fig. S3a. The V 2p orbital exhibits characteristic spin-orbit splitting into two distinct peaks (V 2p_{3/2} and V 2p_{1/2}). Remarkably, both the V 2p and O 1s spectral features - including peak shapes, intensities, and binding energies - remain essentially unchanged throughout the irradiation process.

Quantitative analysis of the binding energies reveals exceptional stability: after 1000 h UV exposure, the measured values for V 2p_{3/2} (516.755 eV), V 2p_{1/2} (524.405 eV), and O 1s (529.755 eV) show negligible deviations (<0.05 eV) compared to both pristine and 500 h-irradiated samples. This rigorous spectroscopic evidence conclusively demonstrates that neither the surface vanadium concentration nor its oxidation state (V⁴⁺) undergoes any measurable alteration.^{1,2} The results provide definitive proof of SVO's outstanding structural integrity, maintaining unchanged surface composition even under prolonged UV irradiation, which underscores its superior oxidation resistance and remarkable UV stability.

Furthermore, comparative analysis of the XRD patterns (Fig. S3b) with different UV irradiation times (0, 500 h and 1000 h) and SEM images (Fig. S3c,d) before and after 1000 h UV irradiation confirm the preservation of both crystalline phase and morphology in SVO. The combined XPS spectral data, XRD patterns and SEM morphological characterization collectively demonstrate that SVO maintains its chemical structure without alteration during UV aging, exhibiting exceptional optical

stability.

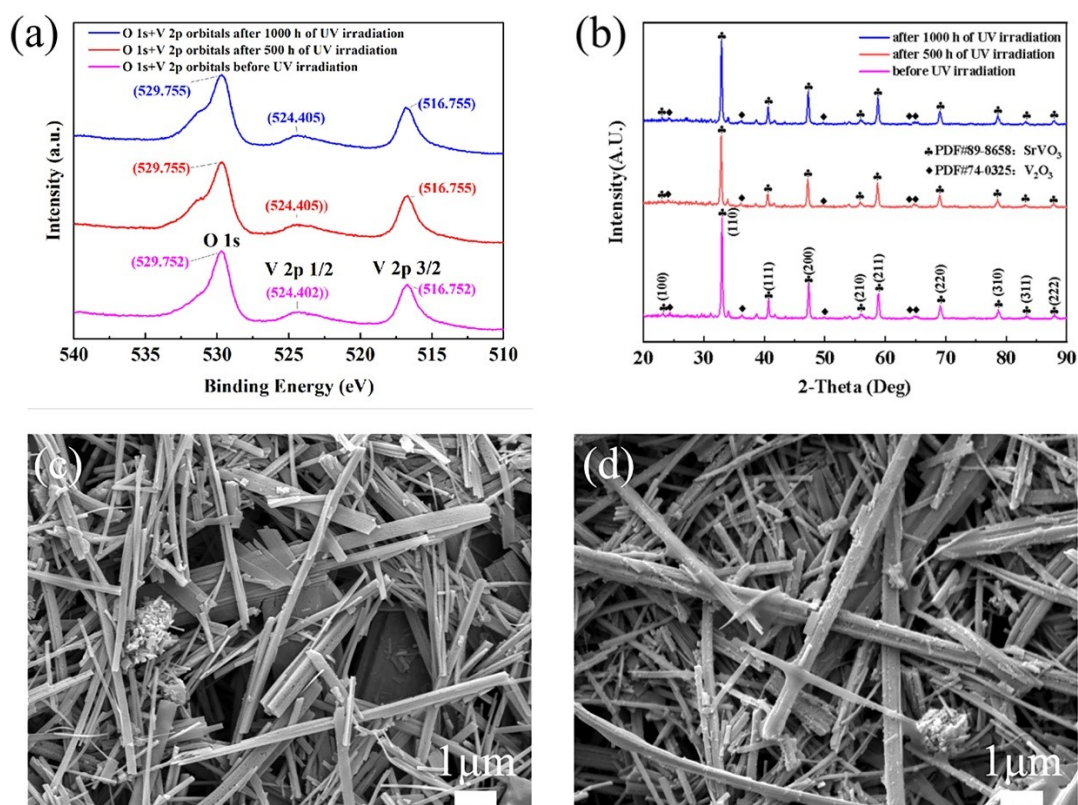


Fig. S3 (a) Overlapping XPS spectra of (O 1s+ V 2p) orbitals of SVO with different UV irradiation times (0,500 h and 1000 h). After 1000 h UV exposure, the negligible binding energy shifts (<0.05 eV) of both V 2p and O 1s orbitals confirm the preservation of V^{4+} oxidation state without further oxidation, demonstrating superior oxidation resistance and UV stability of SVO. (b) XRD patterns of SVO nanofibers with different UV irradiation times (0,500 h and 1000 h). Corresponding SEM images: (c) Pristine and (d) Post-1000 h UV irradiated SVO nanofibers. The XRD patterns and SEM images demonstrate that SVO maintains its chemical structure without alteration during UV aging.

Table S1 Percentage of Ag and S atoms on TCF0, TCF10, and TCFc surfaces before and after UV irradiation test (500 h).

Sample		Ag (At%)	S (At%)
TCF0	before	1.94	0.99
	after	15.14	2.03
TCF10	before	4.11	0.81
	after	4.08	0.92
TCFc	before	6.71	3.04
	after	15.7	5.84

After 500 h UV irradiation, TCF0 and TCFc showed substantial Ag/S percentage increases, while TCF10 exhibited negligible variations, demonstrating SVO-enhanced UV resistance through effective Ag diffusion suppression and ANCL preservation.

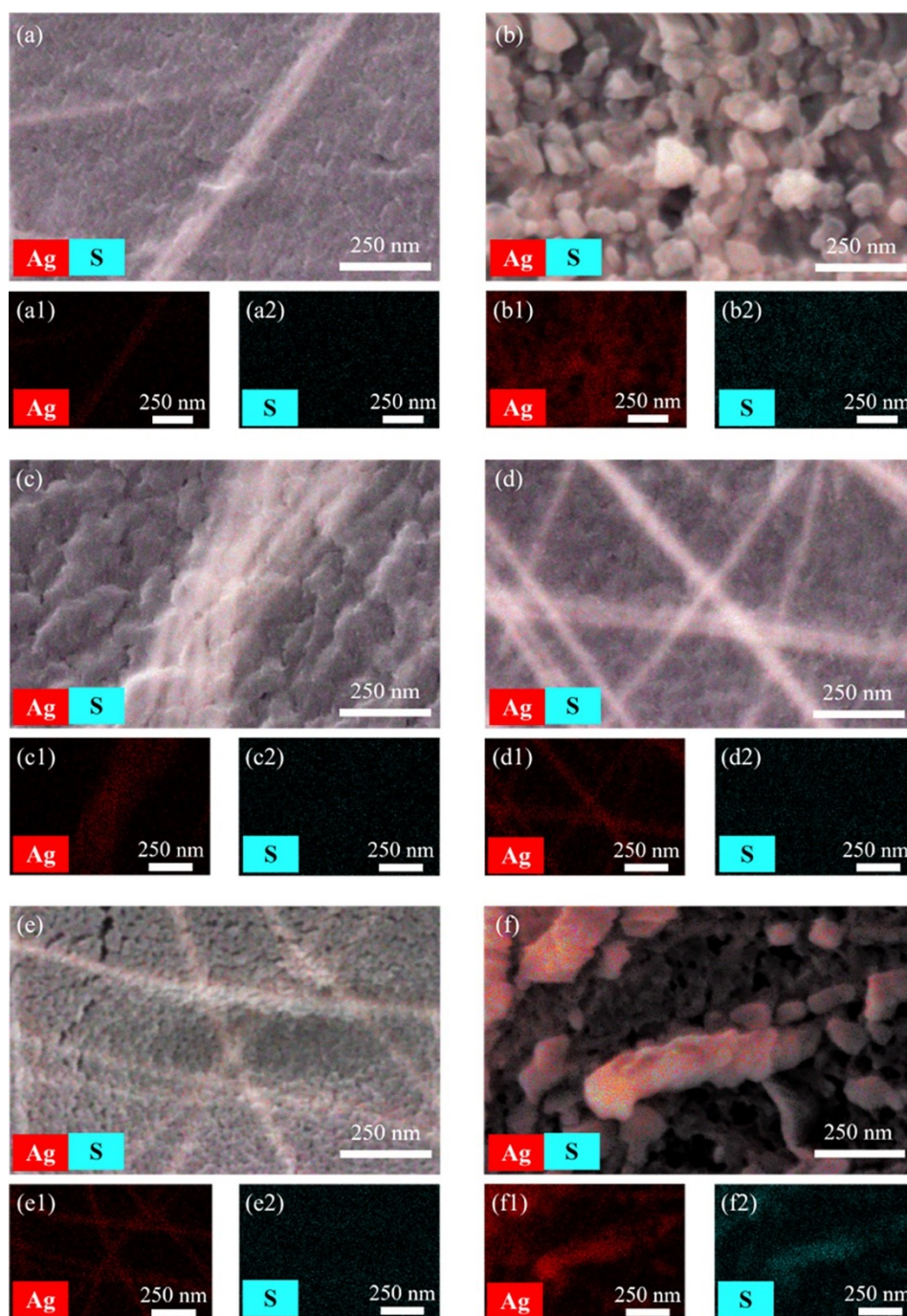


Fig. S4 The combined energy dispersive X-ray spectroscopy (EDS) maps of Ag and S atoms on TCF surfaces before UV irradiation: TCF0 (a, a1, a2), TCF10 (c, c1, c2), TCFc (e, e1, e2), and after UV irradiation (500 h): TCF0 (b, b1, b2), TCF10 (d, d1, d2), TCFc (f, f1, f2). EDS mapping showed UV irradiation (500 h) enhanced Ag signals on TCF0/TCFc surfaces due to severe Ag diffusion/migration, with concurrent S signal enhancement. TCF10 maintained stable Ag/S signals post-irradiation.

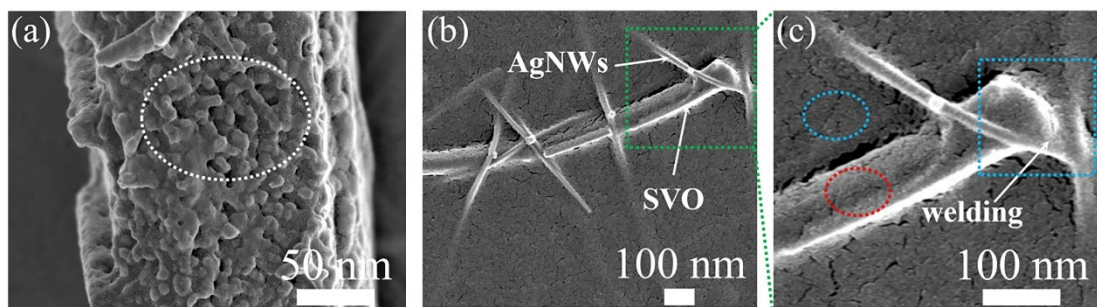


Fig. S5 (a) High-resolution SEM image of the porous SVO surface. (b) SEM micrograph of the welded interface between SVO and AgNWs in TCF10 (highlighted by the green rectangle). (c) Magnified SEM view of the welded SVO-AgNWs interface region. The SVO surface (red circle, Fig. S5c) exhibits identical morphology to the surrounding WPU coating (blue circle, Fig. S5c), lacking porous features (white circle, Fig. S5a). The seamless interface and uniform surface confirm excellent compatibility between substrate, AgNWs, and SVO. Capillary forces induce significant stresses that promote SVO-AgNWs nodal welding, forming an intimate fusion interface (blue rectangle, Fig. S5c). The interface vanishes upon complete fusion (white arrows, Fig. S5c).

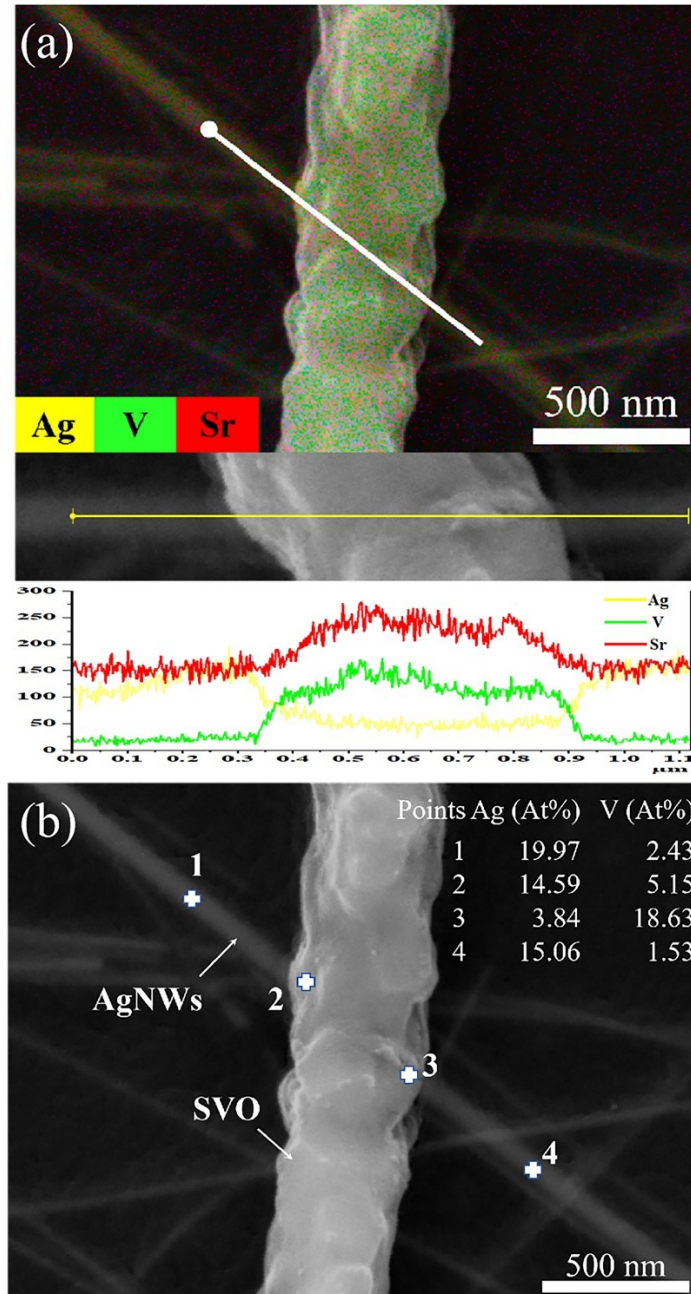


Fig. S6 (a) SEM-EDS line mapping across the interface between an AgNWs and SVO, showing the elemental distribution along the longitudinal axis of the AgNWs. (b) SEM-EDS point mapping at the interfacial region of the AgNWs-SVO junction. The differential distribution of silver atomic signals and Ag atomic percentage near the interfacial region suggests capillary-force-induced diffusion of surface Ag atoms from the AgNWs toward the junction, forming a dense welded interface between SVO and the AgNW that facilitates efficient electron transport.

References

- 1 Y. Bourlier, M. Frégnaux, B. Bérini, A. Fouchet, Y. Dumont and D. Aureau, *Appl. Surf. Sci.*, 2021, **553**, 149536.
- 2 M. Rath, M. Mezhoud, K. O. El, O. Lebedev, J. Cardin, C. Labbe, F. Gourbilleau, V. Polewczyk, G. Vinai, P. Torelli, A. Fouchet, A. David, W. Prellier and U. Luders, *Acs Appl. Mater. Interfaces*, 2023, **15**, 20240-20251.